

Model predictions of the occurrence of non-Maxwellian plasmas, and analysis of their effects on EISCAT data

A. D. FARMER, M. LOCKWOOD

Rutherford Appleton Laboratory, Chilton, Didcot, Oxon OX11 0QX, U.K.

T. J. FULLER-ROWELL

University College London, Gower Street, London WC1E 6BT, U.K.

K. SUVANTO

Blackett Laboratory, Imperial College of Science and Technology, Prince Consort Road,
London SW7 2BZ, U.K.

and

U. P. LØVHAUG

EISCAT Scientific Association, Ramfjordmoen, N-9027 Ramfjordbotn, Norway

(Received for publication 8 December 1987)

Abstract—The recent identification of non-thermal plasmas using EISCAT data has been made possible by their occurrence during large, short-lived flow bursts. For steady, yet rapid, ion convection the only available signature is the shape of the spectrum, which is unreliable because it is open to distortion by noise and sampling uncertainty and can be mimicked by other phenomena. Nevertheless, spectral shape does give an indication of the presence of non-thermal plasma, and the characteristic shape has been observed for long periods (of the order of an hour or more) in some experiments. To evaluate this type of event properly one needs to compare it to what would be expected theoretically. Predictions have been made using the coupled thermosphere-ionosphere model developed at University College London and the University of Sheffield to show where and when non-Maxwellian plasmas would be expected in the auroral zone. Geometrical and other factors then govern whether these are detectable by radar. The results are applicable to any incoherent scatter radar in this area, but the work presented here concentrates on predictions with regard to experiments on the EISCAT facility.

1. INTRODUCTION

Several recent studies have been made of observations of large ion temperature anisotropies (LØVHAUG and FLÅ, 1986), and of non-thermal *F*-region plasmas in the dayside auroral oval (LOCKWOOD *et al.*, 1987, 1988; MOORCROFT and SCHLEGEL, 1988; WINSER *et al.*, 1987). Such plasmas are seen best with EISCAT looking far to the north where the viewing angle approaches perpendicularity with the field line, and identification is clearest when there is a burst of rapid plasma flow as, for example, that expected in the ionospheric signature of a flux transfer event (FTE) occurring at the magnetopause (LOCKWOOD *et al.*, 1987). This is because the changes in spectral width and shape can be unambiguously correlated with the plasma velocity variations, if the time scales are short compared to the time constants for changes in neutral

temperature, winds and ion and neutral compositions. Generally, additional evidence is necessary, as the spectral shape alone is not enough to identify non-Maxwellian plasma. This is because sampling noise, velocity shears and other effects can mimic the spectral shape expected for non-thermal plasma.

While examining such data, however, the spectral shape is a good indicator of periods of interest and for a steady-state or slowly varying atmosphere there may be little other evidence within the data itself to back up the identification. MOORCROFT and SCHLEGEL (1988) and LOCKWOOD *et al.* (1988) have found an anti-correlation of the electron and ion temperatures from spectral fits which assume a Maxwellian ion velocity distribution, and LØVHAUG and FLÅ (1986) and WINSER *et al.* (1987) have noted ion temperature anisotropies which are too great to be satisfactorily explained in terms of a bi-Maxwellian ion velocity

distribution function. Often, though, corroborative evidence is needed to confirm identification of non-Maxwellian plasma. Studies on the data from the UK-POLAR experiment (VAN EYKEN *et al.*, 1984; WILLIS *et al.*, 1986) have shown periods of greater than an hour when the ion flows are exceptionally large and slowly varying (on the time scale of hours) and when the observed spectra are characteristic of non-Maxwellian plasma. It would be difficult to explain such consistent behaviour over such long periods by stochastic (sampling) effects or mixing of Maxwellian plasma species. However, to identify non-thermal plasma unambiguously, some theoretical comparison is needed to show when and where these plasmas are expected.

The theoretical work presented here is in two parts. The first uses models of the upper atmosphere to locate the times and places at which one would expect the plasma to be driven into a non-thermal state. The second part considers the geometric and other conditions determining whether or not measurements with the EISCAT incoherent scatter radar would be affected by the non-thermal nature of the plasma.

This work has two major purposes. First, it is necessary when undertaking some studies of ionospheric behaviour, to be able to exclude any data where there is uncertainty over the calculated parameters. Analysing signals scattered by non-thermal plasma, but making the usual thermal plasma assumption, for example, can lead to significantly incorrect temperatures and sometimes even incorrect densities. Secondly, there is much interest now in studying non-thermal plasmas in their own right; hence a method of pinpointing where data of interest are likely to be found in the vast bank of EISCAT data recorded or yet to be taken will be of value to such studies.

2. PARAMETERISING THE NON-MAXWELLIAN EFFECT

LOCKWOOD and FULLER-ROWELL (1987a, b) have used the University College London–University of Sheffield global, time-dependent, three-dimensional, coupled ionosphere–thermosphere model (FULLER-ROWELL *et al.*, 1984, 1987) to predict the spatial distribution of non-thermal plasma in the *F*-layer. For this work, a parameter had first to be chosen which could be used to quantify and map the non-thermal nature of the plasma.

The parameter chosen is D' , defined as

$$D' = \frac{|\mathbf{v}_i - \mathbf{v}_n|}{(2kT_n/m_n)^{0.5}} \quad (1)$$

It can be seen that this is the ratio of plasma drift velocity (in the rest frame of the neutral gas) to the two-dimensional neutral thermal speed. The use of this parameter is based on considerations of the ion–neutral collision process, which also suggest a ‘critical’ value of D' above which a plasma is detectably non-Maxwellian. ST.-MAURICE and SCHUNK (1979) reviewed ion velocity distributions for a variety of ion–neutral collision models and chose as a simple case for quantitative evaluation the ‘relaxation’ model, where the ion velocity after the collision is assumed to be equal to the neutral particle velocity before. This is a good approximation to a charge-exchange mechanism. They showed that the result of this interaction is that the ions do not have a distribution of field-perpendicular velocities with a width given by their ion thermal temperature, centred on the electromagnetic drift speed $\mathbf{E} \times \mathbf{B}$, as would be observed in the absence of ion–neutral collisions. Instead, the modulus of field-perpendicular velocity is distributed such that its mean is roughly equal to the modulus of the ion–neutral relative velocity, $|\mathbf{v}_i - \mathbf{v}_n|$, and its spread is the thermal spread of the neutrals’ velocities. As a rough guide, ST.-MAURICE and SCHUNK (1979) show that the distribution of field perpendicular velocities has a minimum at the origin (i.e., it is toroidal) if the mean exceeds the spread, i.e. if $D' > 1$, for this relaxation model. Their derivation assumes there are many more neutral particles than ions, and that the ion–neutral collision frequency is much less than the ion gyrofrequency and much greater than the ion–ion collision frequency. That is certainly true between the heights of 200 and 400 km, and probably as far as 600 km.

ST.-MAURICE *et al.* (1976) have found that the form of the distribution function predicted by the relaxation model can be fitted to Retarding Potential Analyser data from the AE-C satellite. In order to do this, however, two empirical fitting factors had to be introduced: the neutral temperature, T_n , was replaced by an effective temperature, T^* , and the ratio D' was replaced by a ‘distribution function deformation factor’, D^* . The exact relationship of D' and D^* is not yet known. MOORCROFT and SCHLEGEL (1988) have calculated the ratio D'/D^* as 0.7, on the basis of the Monte-Carlo simulations of BARAKAT *et al.* (1983). From EISCAT data, LOCKWOOD *et al.* (1988) suggest D' and D^* are roughly equal for D' up to about 1.0, but as D' increases further, D^* tends asymptotically to a maximum of about 1.4.

RAMAN *et al.* (1981), have employed this ‘generalised relaxation model’ to predict the incoherent scatter spectrum for scattering the non-Maxwellian plasma. Examples of the one-dimensional dis-

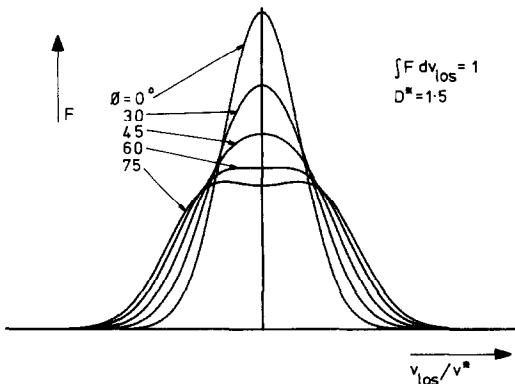


Fig. 1. One-dimensional ion velocity distributions from the generalised relaxation model, F , (see text) for look-directions $\Phi = 0^\circ, 30^\circ, 45^\circ, 60^\circ$ and 75° to the geomagnetic field and a shape factor, D^* , of 1.5. The line-of-sight ion velocities, v_{los} , are normalised to $v^* = [(2kT_i/m_i)/(1 + \frac{2}{3}D^{*2})]^{0.5}$, where T_i is the 3-dimensional ion temperature.

tributions of line-of-sight ion velocities, F , for different aspect angles, Φ , and $D^* = 1.5$, are shown in Fig. 1. These distributions have been evaluated for the RAMAN (1981) distribution function using the analytic procedure by SUVANTO (1987), and are shown as a function of (v_{los}/v^*) where $v^{*2} = (2kT_i/m_i)/(1 + \frac{2}{3}D^{*2})$ and T_i is the three-dimensional ion temperature. For $D^* = 0$ there is a Maxwellian distribution for all look directions, but for $D^* > 0$ the distribution is only Maxwellian for $\Phi = 0$ (i.e. along the magnetic field). Figure 1 shows that F has a flatter maximum than a Maxwellian for $D^* > 0$ and $\Phi > 0$, and has a slight minimum at the origin for $\Phi \geq 70^\circ$ (i.e., it is a weakly toroidal distribution function). Note that the suggestion by LOCKWOOD *et al.* (1988) that D^* may have a maximum of 1.4 means, therefore, that the plasma would be, at most, only weakly toroidal.

For the relaxation model and the other simple ion neutral collision models used by ST-MAURICE and SCHUNK, one would expect to see departures from Maxwellian ion velocity distribution functions for D' as low as 0.75. Other studies have refined this, however, by including more realistic models of ion-neutral collisions. One can include, for example, polarisation elastic scatter and true resonant charge-exchange interactions. The first of these causes scatter of field-perpendicular velocities into velocities parallel to the magnetic field and so acts to destroy the toroidal form predicted for the simple relaxation process. BARAKAT *et al.* (1983) have simulated a mix of these two processes and shown that the effect is to raise the D' threshold for the onset of a toroidal

distribution compared to that for the simple relaxation case. Thus, instead of toroidal distributions occurring when $D' > 1$, one needs D' around 1.5–2.

A further complication is that instabilities develop at higher values of D' , driven by, and tending to destroy, the toroidal distribution. The most well-known is the so-called 'Post-Rosenbluth' instability. Indeed, instabilities may even prevent the formation of toroidal distributions (and therefore raise the D' threshold for their formation to infinity). However, simulations by RAMAN *et al.* (1981) show that non-Maxwellian effects should be observed by incoherent scatter radars at lower D' than the threshold for producing toroidal distributions. The flattened Maxwellians shown in Fig. 1 are sufficient for detection at look directions which make an angle, Φ , as low as 45° to the magnetic field. Experimental evidence suggests that the D' threshold for observing non-Maxwellian plasma by incoherent scatter at larger Φ is close to 1.0; LOCKWOOD *et al.* (1987, 1988) found non-thermal plasma in flow bursts whenever D' exceeded 1.0 for $\Phi = 73.5^\circ$. MOORCROFT and SCHLEGEL (1988) have estimated D' may be near 1.3 in their observations of non-thermal plasma at somewhat lower angles.

3. MODEL PREDICTIONS

To calculate D' we need v_n , v_i , T_n and m_n . These were obtained from the three-dimensional coupled thermosphere-ionosphere model mentioned above. In this, the momentum input for the ions comes mainly from the electric field generated across the polar cap by the interaction of the Earth's magnetic field with the solar wind. A model of this 'convection' electric field has to be supplied, and for the results shown below two Heppner models, A-2 and B-2 (as illustrated in REES *et al.*, 1986), were used. They are shown in Fig. 2, in the MLT-invariant latitude frame. The A-2 and B-2 patterns are used in the modelling work for the northern and southern hemispheres, respectively, to simulate conditions where the interplanetary magnetic field (IMF) B_y component is negative. In this paper these models are used with a cross-cap potential of 76 kV (as shown in Fig. 2) or 152 kV. However, the radius and centre of the polar cap are not varied, hence the cap boundary is always at the locations shown in Fig. 2 and the equipotential contours always have the same pattern.

The UCL-Sheffield University model gave the results shown in Figs. 3, 4 and 5. These are all for December (winter solstice), a solar flux $F_{10.7}$ index of 185 and with TIROS activity level 7 and a cross-cap potential of 76 kV ($Kp \sim 3$). They cover geographic

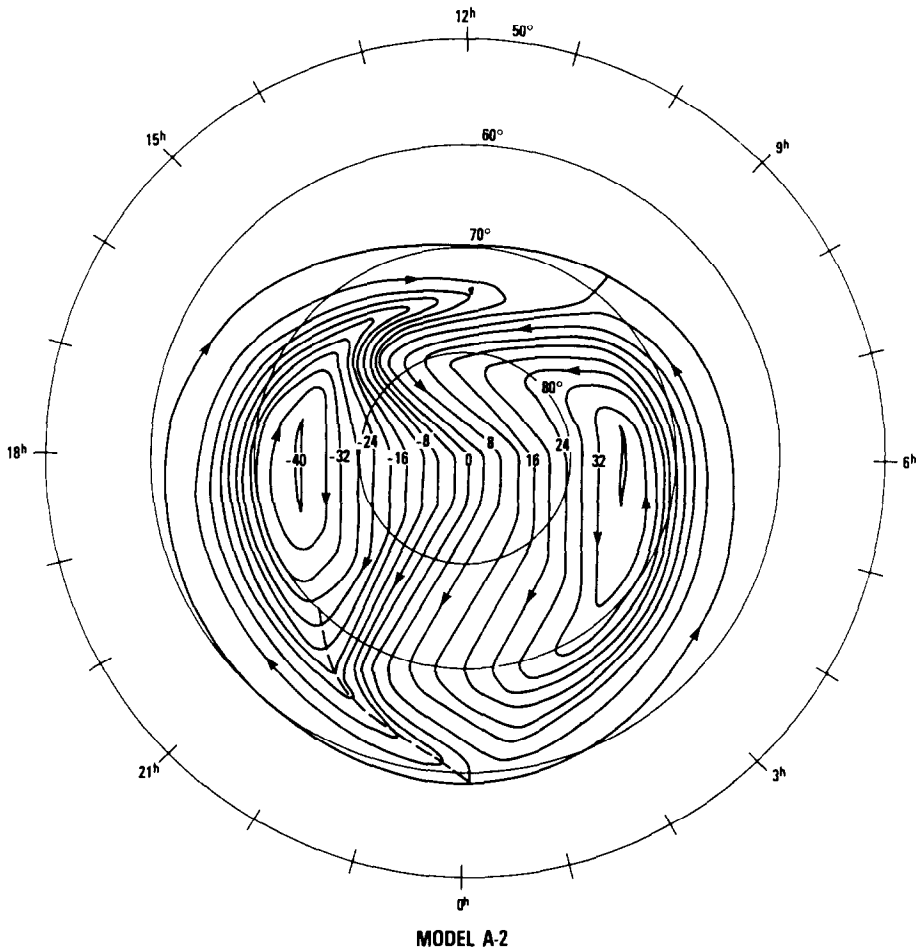


Fig. 2. Heppner and Maynard models of the electric potential distribution in the high latitude ionosphere. In the modelling employed in this paper, the A-2 model (above) is used in the northern hemisphere with the B-2 model (opposite) in the southern in order to simulate IMF $B_y < 0$ conditions.

latitudes 50° – 90° north and show the results obtained when the model has been left to run until steady-state has been achieved in a diurnal sense.

Figure 3 is a colour plot of the values of D' for NO^+ ions at a constant pressure level corresponding roughly to 200 km height and for a longitude of 18° east, near to that of EISCAT. (Tromsø is at 19.23° .) This is not a 'snapshot' of the northern hemisphere, but an illustration of the conditions seen at this longitude through a 24 h period. The top diagram shows contours of D' in an x - y plot of latitude vs. UT. The bottom diagram is this same data repeated in a polar dial form, where the times marked are SLT. (Note 1200 SLT is at the bottom of the plot. SLT is Solar Local Time, and is calculated as $\text{UT} + \text{longitude}/15$, where SLT and UT are in decimal hours and longitude

is measured eastwards in degrees.) It is seen that the maximum values of D' occur in the cusp around 06–10 SLT (at around 80° geographic latitude) and within the auroral oval around and after local midnight and, to a lesser extent, 1200–1500 LT. The peak value of D' is 1.195 in the cusp, and there is an area covering 3–4 h of SLT where D' is at or near 1.0. This latter region corresponds to the dawn sector auroral oval in an MLT-invariant latitude plot.

Figure 4(d) is a contour plot of D' , this time showing a 'snapshot' of the northern hemisphere at 18 UT (EISCAT thus being at about 1930 SLT). Note the differences between Fig. 3 and 4d, which give some idea of the different patterns that would be seen by radars such as Sondrestrom and Millstone Hill at different longitudes, due to the effect of the offset of

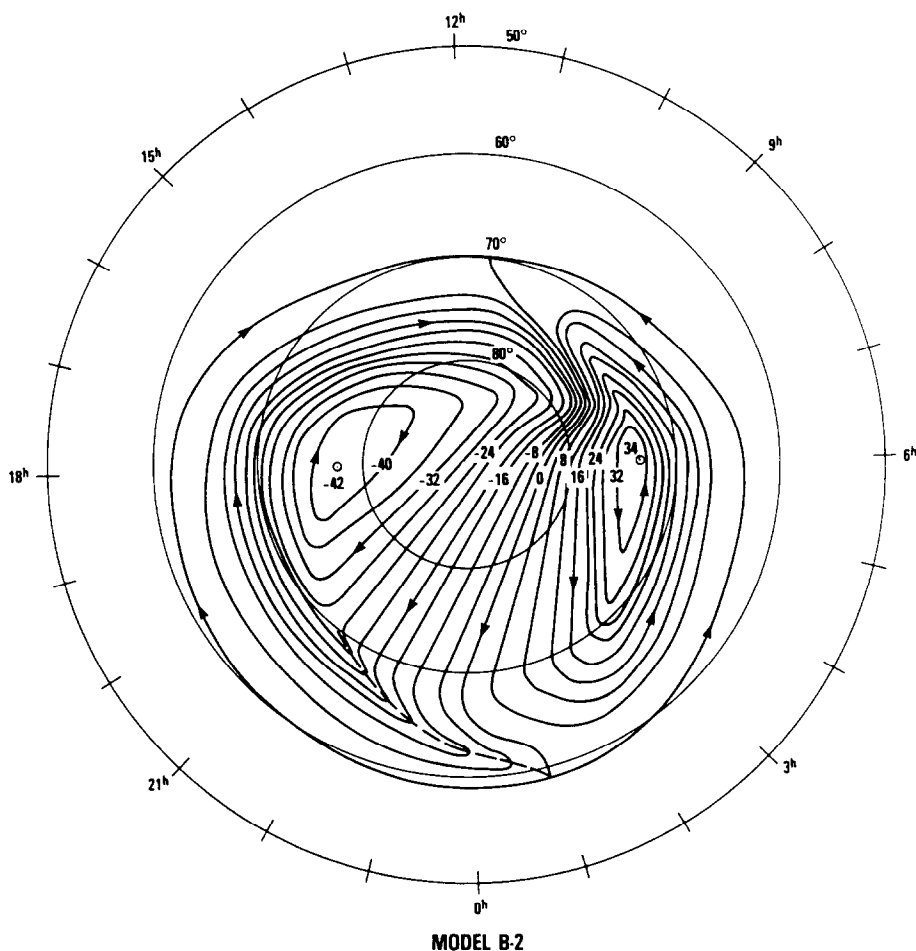


Fig. 2.—continued.

the geomagnetic and geographic poles. Figure 4 also shows the input ion convection velocities (transformed into the geographic latitude–SLT frame at this UT; see Fig. 4a), and the modelled neutral velocities (Fig. 4b), and neutral temperatures (Fig. 4c). Equation (1) shows that the maximum values of D' will occur where the ion and neutral velocity vectors differ most. There is a significant difference between the ion and neutral flow patterns. Both are two-celled, with a clockwise rotating cell on the dusk side and a counter-clockwise cell on the dawn side; however, the ion flows are more clearly symmetric than the neutral flows. The ion flows in the dawn and dusk sectors of the auroral oval are of roughly equal speeds, whereas the neutral winds are much smaller near dawn than dusk.

The dawn–dusk asymmetry in auroral neutral wind speed arises because the neutral air in the dawn sector of the auroral oval is subject to a coriolis force and a

curvature effect which act in the same sense, so that a packet of neutral air tends to move equatorward out of the region where it is accelerated by the ion drag. Conversely, in the dusk cell the effect of curvature and the coriolis force are opposed and so largely cancel, and the neutral air 'packets' stay in the auroral oval long enough to pick up a large amount of sunward momentum from the large ion flows. Further details of this asymmetry and relevant observations have been discussed by LOCKWOOD and FULLER-ROWELL (1987a).

Figure 5 shows the values of D' for O^+ at a constant pressure level near 300 km, in the same format and under the same conditions as Fig. 3. It can be seen that the distribution of D' is very similar to that in Fig. 3, but D' values are somewhat lower for the O^+ case. However, the locations of the maxima and the extent of the regions of high D' are much the same.

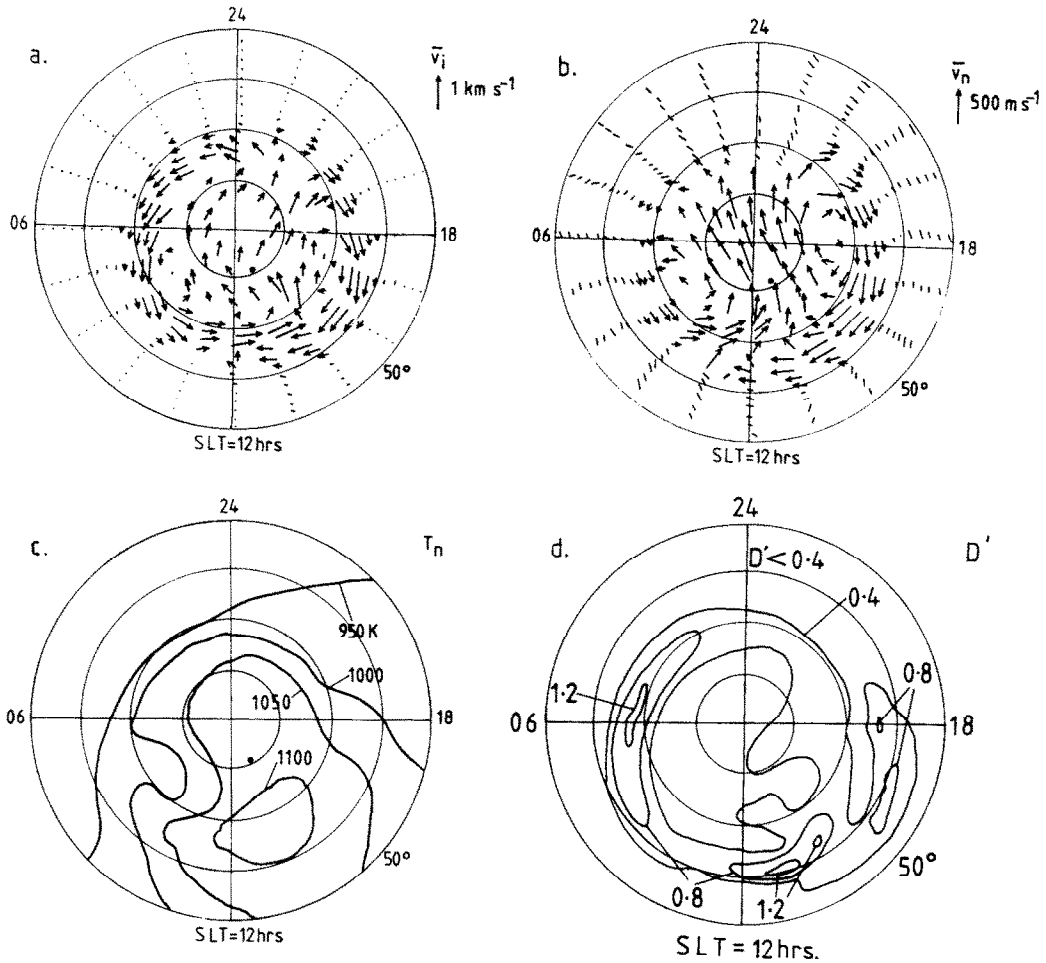


Fig. 4. Predictions from the UCL–Sheffield University coupled model for 18 UT and the same geophysical conditions as Fig. 3. (a) The ion velocity vectors, \bar{v}_i ; (b) the neutral wind vectors, \bar{v}_n ; (c) the neutral temperature, T_n ; and (d) the ratio D' for NO^+ at roughly 200 km altitude. All plots are polar dials as a function of geographic latitude (over the range 50° – 90°) and Solar Local Time (SLT).

Note that the latitudes of the regions of high D' would be different for a different size polar cap.

Figure 6 presents the predictions for NO^+ at 200 km in the same format as Fig. 4d, but showing the situation immediately following an increase in cross-cap potential from 76 kV to 152 kV at 18 UT (the other geophysical conditions staying the same as for Figs. 3, 4 and 5). The use of the word ‘immediately’ implies that the ion velocities have responded to the increased electric field, but the neutrals have not, so that there is an extra difference between ion and neutral velocities. The polar cap and convection pattern have not had time to expand in response to the increased cross-cap potential in the manner described by LOCKWOOD *et*

al. (1986a, b). Gradually (on time scales of tens of minutes to hours) ion drag will cause the neutral atmosphere to respond and the ‘steady-state’ then reached (if the potential stays high) will be one where the neutral wind velocity is greater overall and where the polar cap convection pattern has expanded.

Comparison of Figs. 4d and 6 shows that the effect of the greatly increased ion–neutral velocity difference is to increase D' , but without greatly affecting the spatial distribution of D' . The peaks in Fig. 6 are for $D' > 2.4$ around 0600 and just after 1200 SLT in the oval, as in Fig. 4d. The pattern will later relax back to smaller values of D' for an expanded pattern of convection (although it will not return completely to

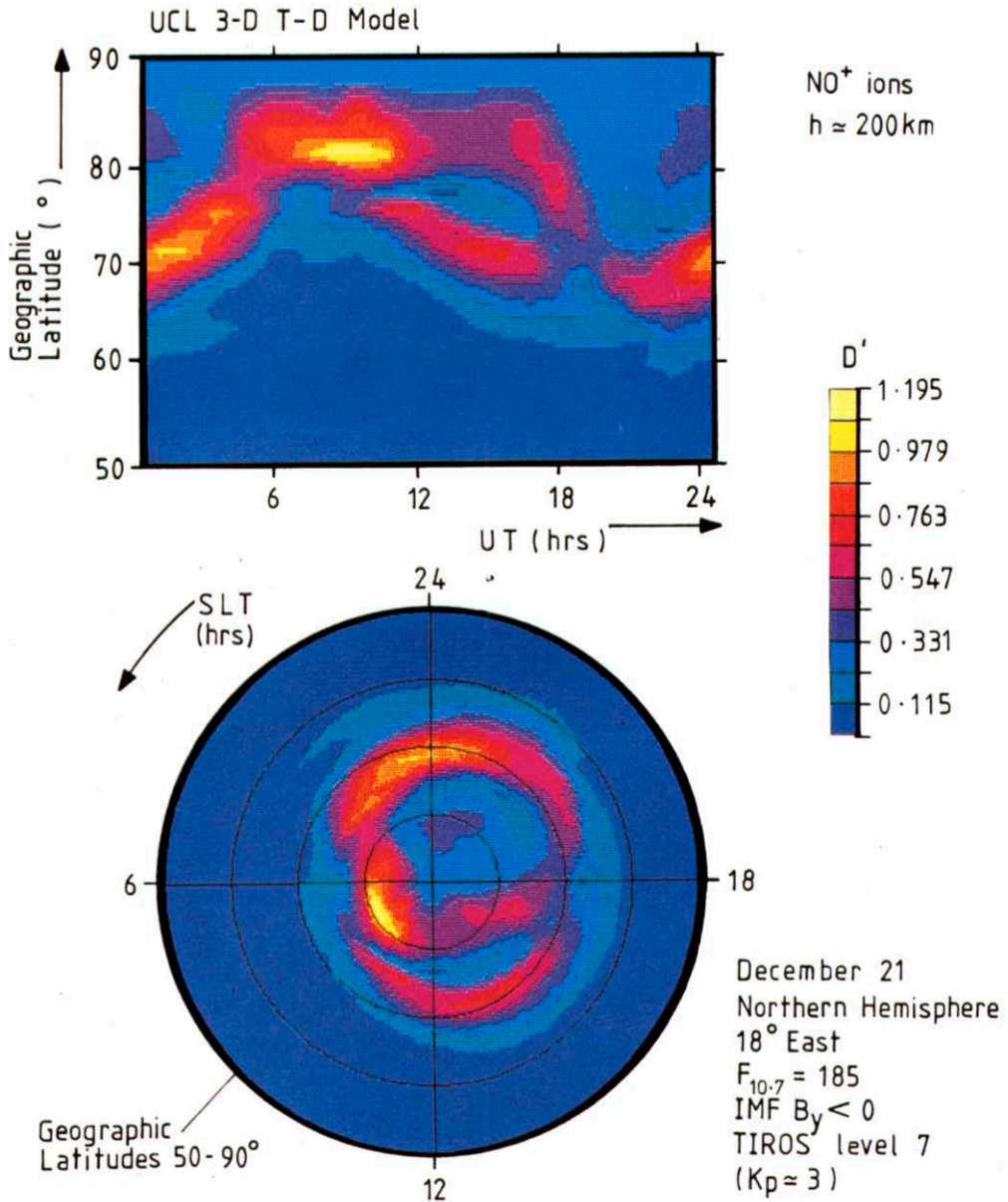


Fig. 3. The ratio D' for NO^+ ions at a constant pressure level at approximately 200 km (see text). The top panel shows D' as a function of geographic latitude and Universal Time and the lower panel shows D' in a geographic latitude–Solar Local Time (SLT) polar dial format. All data are for the northern hemisphere at 18° east and are for December solstice with $F_{10.7} = 185$, IMF $B_y < 0$, a cross-cap potential of 76 kV and TIROS auroral activity level of 7 ($K_p \sim 3$). This is for the relaxation model $D^* = D'$.

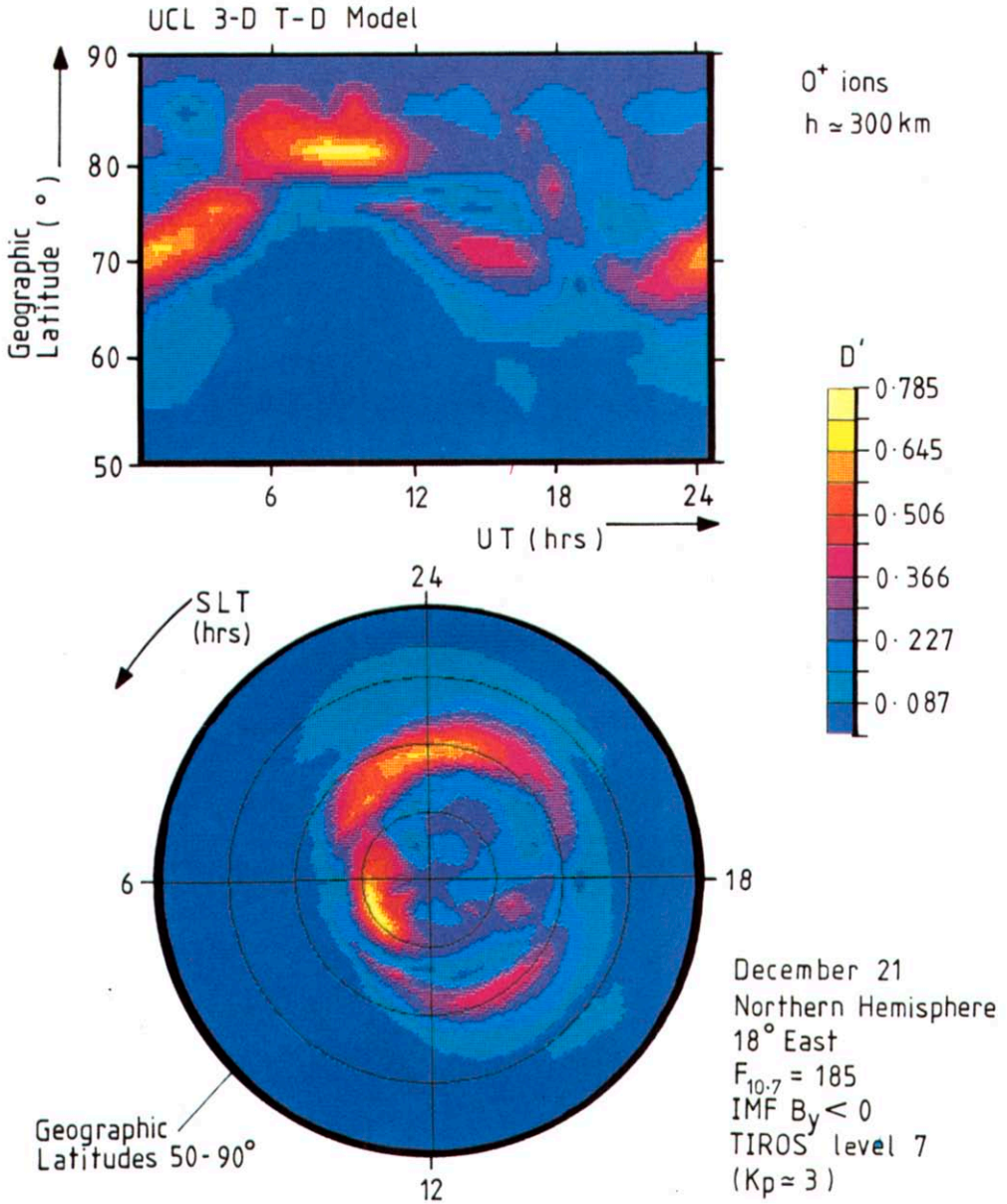


Fig. 5. As Fig. 3, but for O^+ ions at a constant pressure level at approximately 300 km.

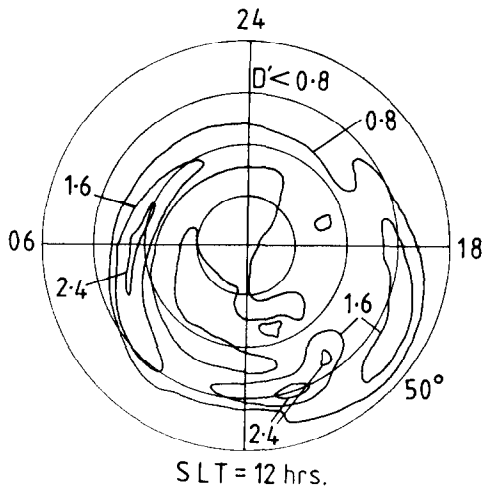


Fig. 6. Predictions of D' for NO^+ at 200 km in the same format as Fig. 4d and immediately following an increase in cross-cap potential from 76 to 152 kV at 18 UT. The other geophysical conditions are the same as for Figs. 3, 4 and 5.

the situation of Fig. 4d as long as the cross-cap potential remains high).

Therefore, we can conclude that, at low to medium activity levels there are regions, even for steady-state conditions, where non-Maxwellian plasma will occur, in particular in the post-midnight sector of the auroral oval and in the cusp. Also, they are more likely to be found in the NO^+ -dominated, rather than at O^+ -dominated, heights. Any transient activity, such as a flux transfer event or an increase of convection on time scales of hours (e.g. due to substorms or sudden increases in cross-cap potential), will often give enough extra ion velocity to drive the plasma into a non-thermal state over much greater regions, and the regions of maximum D' identified on the 'steady-state' plots (Figs. 3–5) will then contain plasma which deviates from Maxwellian by an even greater extent.

4. DETECTION BY EISCAT

Whether a region of non-thermal plasma is detectable by EISCAT will depend on a number of factors. The most obvious ones are the distance and orientation of the region from the radar: there will be a maximum useful range given by factors such as the radar power and gain (MURDIN, 1979) and there may be elevation or azimuth restrictions on the radar's movements. Another factor is the spectral shape of the detected signal. For example, non-Maxwellian plasmas with a low electron temperature will be a lot harder to distinguish from Maxwellian plasmas than those with a high electron temperature (see spectra

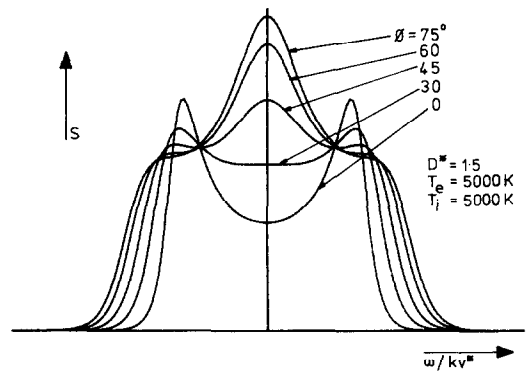


Fig. 7. Incoherent scatter spectra for the generalised relaxation model with $D^* = 1.5$ and equal electron and 3-D ion temperatures of 5000 K, for aspect angles, Φ , of 0° , 30° , 45° , 60° and 75° . The corresponding line-of-sight ion velocity distributions are given in Fig. 1. The phase speeds are normalised to v^* .

simulated by RAMAN *et al.*, 1981; HUBERT, 1984).

The aspect angle of the radar look-direction with respect to the magnetic field direction, Φ , is also critical in identifying the non-thermal plasmas by their radar spectra. This is shown by Fig. 7, from the algorithm of SUVANTO (1987), based on the work of RAMAN *et al.* (1981). Figure 7 shows the spectra seen by an incoherent scatter radar (ISR) looking at a non-Maxwellian plasma at different angles to the magnetic field. This is for the generalised relaxation model with $D^* = 1.5$, so that the corresponding line-of-sight velocity distributions are given in Fig. 1. For look directions close to parallel to the field line ($\Phi < 30^\circ$) one sees the standard 'double-humped' spectrum, as the line-of-sight distribution is close to Maxwellian. As the angle to the magnetic field increases, the spectrum develops a central peak, which grows larger than the shoulders of the Maxwellian spectrum until it eventually becomes dominant.

WINNER *et al.* (1987) have observed the aspect angle dependence of the spectrum described by Fig. 7 using EISCAT. Experiments looking near-parallel will not be able to distinguish non-Maxwellian from Maxwellian plasma (at least for the forms of distribution function predicted for large ion drifts in the presence of ion-neutral collisions). The aspect angles at which the spectrum is distorted enough to be detectably different from the Maxwellian case will depend somewhat on the noise level in the data, but from $\Phi = 45^\circ$ – 60° to perpendicularity is roughly the range over which high D' (giving high D^*) affects the spectrum significantly. An aspect angle of 54.7° has particular significance, as above this D' in the range $1 < D' < 2$ (as predicted in the previous section) will certainly cause an ISR to

overestimate ion temperature. This is due to the effects of both anisotropic and non-Maxwellian distribution functions (see discussion given by LOCKWOOD *et al.*, 1988). The angle 54.7° is that at which the line-of-sight temperature T_r is equal to T_i , where $T_i = (T_\perp + 2T_\parallel)/3$. T_\perp and T_\parallel are the effective temperatures perpendicular and parallel to the magnetic field.

Thus, we can consider the geometries of various EISCAT experiments in conjunction with the ionosphere–thermosphere model predictions presented in the previous section, to determine in which regions, and when, one would expect to be able to detect non-Maxwellian spectra. Using a standard magnetic field model one can plot the angle Φ with respect to B for different EISCAT experiments and note where that angle is greater than, for example, 54.7° .

In the EISCAT field-of-view (MURDIN, 1979), the magnetic field is inclined to the south (e.g. at Tromsø it is at an angle of about 13.5° from vertical, approximately in the meridian plane). Thus, to make measurements at the largest possible angle to B one has to operate the radar at low elevation angles. For any given elevation, the angle to the field is larger in the north than south. Mountains near the transmitter at Tromsø restrict elevations to values above 15° – 19° , so the beam can never reach full perpendicularity.

For the remote sites (Kiruna and Sodankylä), the received spectrum is sensitive to the ion velocities along a direction which is the bisector of the angle subtended by transmitter and receiver beam directions. At large elevation angles from Tromsø this bisector is near vertical. To the south of Tromsø, the bisector (for both Kiruna and Sodankylä) subtends a smaller angle to the field line than the Tromsø beam. Only north of Tromsø do the remote sites have a measurement direction which is at a greater angle to the field line than for Tromsø. At very low elevations, because one only gets signal return above 80 km height, useful signal will only come from long ranges, and then all three sites' beams will tend to be at more or less the same aspect angle. Overall, then, for EISCAT, one can concentrate on evaluation of the geometry from Tromsø, knowing that the remote sites are not likely to detect non-thermal spectra where Tromsø cannot. This is not to say that studies of the difference in measurements between Tromsø and the remote sites are not useful; LÖVHIAUG and FLÅ (1986), for example, used the differences in ion temperature (deduced with the assumption that the plasma is Maxwellian), T_{ms} , measured at the different sites (due to the different aspect angles with respect to the field line) to demonstrate anisotropies during substorms.

Effect on common programme CP-3

Figure 8 shows contours of the Tromsø aspect angle, i.e., the angle subtended by the Tromsø beam with the Earth's magnetic field, for the meridian plane through Tromsø. The field calculations are based on the IGRF80 model. Also shown are the projections onto this plane of the scan positions of CP-3-E. (This 'projection' may introduce errors of up to 2° or 3° in apparent aspect angle at the lowest elevations, since the CP-3-E scan actually makes an angle of around 12° with the meridian.) As expected, the greatest angles with respect to the field are subtended to the north, where one comes to within about 16° of perpendicularity. To the south, the lowest scan position barely reaches 65° off the field line near to the radar. At the farther ranges the maximum is 50° or less. Hence, as expected, CP-3 will be subject to the effects of non-thermal plasma when looking into the same regions as observed by UK-POLAR (VAN EYKEN *et al.*, 1984; WILLIS *et al.*, 1986). In Section 5 we review some of the EISCAT observations from these two experiments which have already been used to prove or infer the presence of non-Maxwellian plasma.

The scan positions 1–5 of CP-3-E give aspect angles exceeding 54.7° , and this occurs in the height range where non-thermal plasma is expected (~ 200 – 600 km, i.e., between the horizontal dashed lines in Fig. 8) in the geographic latitude range 73 – 80° . Usually CP-3 observations do not reach a latitude anywhere near the upper limit, as signal strengths are too low. Figures 3 and 5 therefore show that CP-3-E should detect non-thermal plasma in the dawn auroral oval between about 0 and 6 UT (for scan positions of about 5 or lower and at heights above about 200 km) for the conditions used to derive Figs. 3 and 5. Note that the moderate D' at the required latitudes between about 11 and 15 UT in the afternoon sector may often increase above the detection threshold during increases in convection strength (Fig. 6). The very high values of D' in the cusp region are beyond the latitude range of this experiment under all but the most exceptional circumstances.

Also shown on Fig. 8 are the elevation scan limits for the VHF system at Tromsø (30° and 120° from north). To the north, the largest aspect angle to the magnetic field possible with this system is around 60° , which means experiments are unlikely to be so greatly affected by non-Maxwellian plasmas except under exceptional circumstances. In the south the largest aspect angle is around 25° , and Fig. 7 demonstrates that this is inadequate to give strong non-thermal effects.

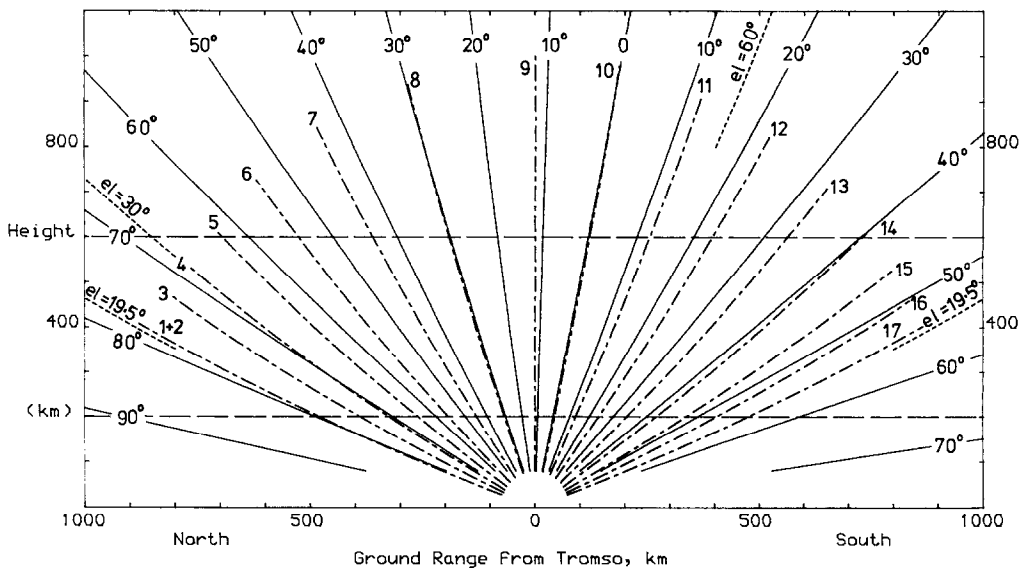


Fig. 8. The orientation of the Earth's magnetic field in the meridian plane through Tromsø. The solid curves give the aspect angle, Φ , and the chained curves the beam directions for EISCAT programme CP-3-E, projected onto the same plane and plotted as a function of altitude and ground range. The elevation scan limits of the EISCAT UHF and VHF systems are also shown; i.e., 19.5° north and south for the UHF, and 30° to the north, 60° to the south for the VHF.

5. SOME EISCAT RESULTS TO DATE

Non-Maxwellian spectra were first identified in incoherent scatter data using the UK-POLAR experiment. The unambiguous identification was made possible by rapid, short-lived flow bursts (LOCKWOOD *et al.*, 1987). However, there are many examples of spectra characteristic of non-Maxwellian plasma in the UK-POLAR data which persist for much longer periods. Figure 9 shows an example of some data from 2 h of the UK-POLAR experiment. During rapid but steady flow conditions, persisting for over an hour, the spectra are seen to change from a Maxwellian, double-humped form to central single-peaked form, such as one would expect with a highly non-Maxwellian plasma (see Fig. 7 which is for $T_e = T_i = 5000$ K). The second panel shows the spectra, as 5 min averages (one in each 10 min beamswinging cycle), and below them the corresponding average vector ion velocities and velocity magnitudes derived from the beamswinging technique. At the top of the figure are the signal-to-background noise ratios. These data are taken looking at an azimuth of 356° from Tromsø, at an altitude of 243 km.

The UT and latitudes at which the non-thermal shaped spectra are observed are consistent with the predictions shown in Figs. 3–6. Figure 9 shows that the ion velocities are exceptionally large, being over

2 km s^{-1} for more than an hour and peaking at 3 km s^{-1} near 00 UT. The reasons for these very high flows are understood when data from the Sondrestrom radar, taken during a combined experiment on this day, are considered with the EISCAT data. LOCKWOOD *et al.* (1986a), have shown that there was a very large increase in cross-cap potential at about 19 UT. Hence these data would be an example of the kind shown in Fig. 6, where the plasma in a region of moderately high D' under quiet conditions is driven into a highly non-thermal state by an increase in polar cap potential.

MOORCROFT and SCHLEGEL (1988) have presented a polar dial plot of the locations of CP-3 observations of high apparent ion temperature, T_{ims} , as a function of SLT and geographic latitude, i.e. in a similar format to the lower panels of Figs. 3 and 5. They show that the occurrence of high T_{ims} , a probable indication that the assumption of a Maxwellian distribution is incorrect, has a distribution closely following the predictions of Figs. 3 and 5. The cusp (0600–0900 SLT) peak of Figs. 3 and 5 is missing because it is beyond the range of the radar. Hence these initial results are very similar to those expected from the discussion in the previous section, but it should be noted that statistics are poor, as the study does not yet contain sufficient days of observation.

The Moorcroft and Schlegel results are for a mix

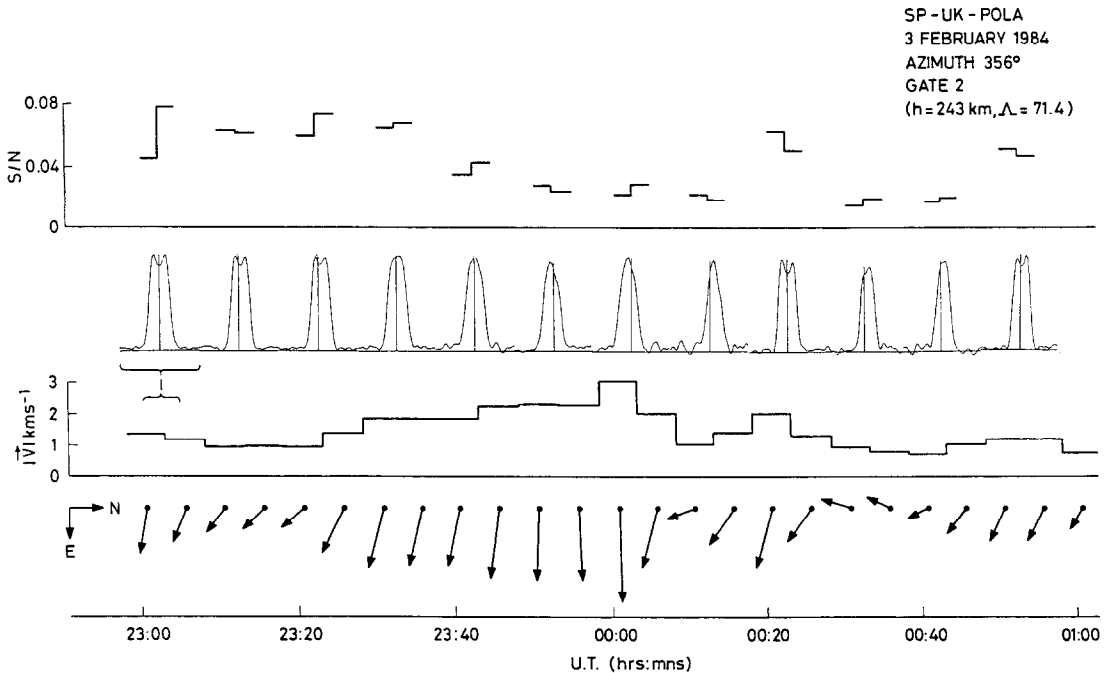


Fig. 9. Example of EISCAT UK-POLAR data indicating the presence of non-thermal plasma for more than an hour. The bottom panel shows the ion flow vectors (plotted with northward to the right of the figure), above which are shown the velocity magnitudes $|v_i|$, deduced by the beamswinging technique. The top panel shows the received signal-to-background noise ratio below which are given the 5 min post integrated spectra. All data are for the azimuth 356° and UK-POLAR gate 2, for which the altitude is 243 km and the invariant latitude is 71.4° .

of different activity levels. Steady-state conditions probably apply to a minority of the cases, since the orientation of the interplanetary magnetic field with respect to the Earth's field is highly variable, and the high-latitude flows may essentially be in a continual state of transition from one pattern to another under its influence. The work presented here, however, although based on the assumption of a steady-state, has been shown to have legitimate applications to non-steady-state conditions. Moorcroft and Schlegel do find several incidences of high T_{im} in the afternoon sector, which we would therefore explain in terms of time-dependent convection enhancements (as in Fig. 6). Non-thermal shaped spectra have been observed in association with convection enhancements in the afternoon sector by WINSER *et al.* (1987), using CP-3 and also in UK-POLAR data (LOCKWOOD *et al.*, private communication). Unreasonably high temperature anisotropies, deduced by assuming a bi-Maxwellian distribution function, have also been reported following substorms by LØVHAUG and FLÅ (1986), indicating non-Maxwellian plasma.

CONCLUSIONS

By modelling the behaviour of the coupled ionosphere-thermosphere system we can predict, in the form of contours of D' (the ratio of the difference between the ion and neutral velocities to the two-dimensional neutral thermal speed) the regions and times for which the ion velocity distribution is most likely to be (or approach) a non-Maxwellian form. A value of D' of $0.75\text{--}1.0$ seems to be the critical level for non-thermal effects on incoherent scatter observations at large aspect angles. For low to medium magnetic activity levels, the ionosphere is mostly below this threshold, though one might see exceptions in data taken by the UHF system in the cusp at 80° latitude and in the post-midnight auroral oval. For high Kp and in transient situations (which may well apply for the majority of the time) we would expect to find such plasmas more often and we can use the steady-state predictions to indicate the most likely regions for this.

Non-thermal ion distributions will be most easily

detectable by an ISR radar such as EISCAT at places where the beam direction makes a large angle with the field line. By considering this in conjunction with the D' predictions, one can determine where for each experiment, if at all, one is most likely to find non-thermal effects. This is useful either if one wishes to identify and reject data for which the analysis with the 'usual' Maxwellian assumptions is erroneous, or if one is specifically studying non-thermal plasma effects.

Acknowledgements—The authors are grateful to the many scientists at UCL and Sheffield University who have assisted in the development of the model and to D. M. WILLIS for his comments on this manuscript. We also thank the director and staff of EISCAT for their help. EISCAT is supported by the British SERC, French CNRS, West German MPG, Norwegian NAVF, Swedish NFR and Finnish SA. K.S. is supported by the Oskari Huttunen Foundation in Finland, and an ORS scholarship, with assistance from the Academy of Finland. TJFR is supported by a SERC Advanced Fellowship.

REFERENCES

- BARAKAT A. R., SCHUNK R. W. and ST.-MAURICE J.-P. 1983 *J. geophys. Res.* **88**, 3237.
- VAN EYKEN A. P., RISHBETH H., WILLIS D. M. and COWLEY S. W. H. 1984 *J. atmos. terr. Phys.* **46**, 635.
- FULLER-ROWELL T. J., REES D., QUEGAN S., BAILEY G. J. and MOFFETT R. J. 1987 *J. geophys. Res.* **92**, 7744.
- FULLER-ROWELL T. J., QUEGAN S., REES D., BAILEY G. J. and MOFFETT R. J. 1984 *Planet. Space Sci.* **32**, 469.
- HUBERT D. 1984 *J. atmos. terr. Phys.* **46**, 601.
- LOCKWOOD M. and FULLER-ROWELL T. J. 1987a *Geophys. Res. Lett.* **44**, 371.
- LOCKWOOD M. and FULLER-ROWELL T. J. 1987b *Geophys. Res. Lett.* **14**, 581.
- LOCKWOOD M., VAN EYKEN A. P., BROMAGE B. J. I., WAITE J. H. JR., MOORE T. E. and DOUPNIK J. R. 1986a *Adv. Space Res.* **6**, 93.
- LOCKWOOD M., VAN EYKEN A. P., BROMAGE B. J. I., WILLIS D. M. and COWLEY S. W. H. 1986b *Geophys. Res. Lett.* **13**, 72.
- LOCKWOOD M., BROMAGE B. J. I., HORNE R. B., ST.-MAURICE J.-P., WILLIS D. M. and COWLEY S. W. H. 1987 *Geophys. Res. Lett.* **14**, 111.
- LOCKWOOD M., SUVANTO K., ST.-MAURICE J.-P., KIKUCHI K., BROMAGE B. J. I., WILLIS D. M., CROTHERS S. R., TODD H. and COWLEY S. W. H. 1988 *J. atmos. terr. Phys.* **50**, 467.
- LØVHAUG U. P. and FLÅ T. 1986 *J. atmos. terr. Phys.* **48**, 959.
- MOORCROFT D. and SCHLEGEL K. 1988 *J. atmos. terr. Phys.* **50**, 455.
- MURDIN J. 1979 EISCAT Technical Note 79/16.
- RAMAN R. S. V., ST.-MAURICE J.-P. and ONG R. S. B. 1981 *J. geophys. Res.* **86**, 4751.
- REES D., FULLER-ROWELL T. J., GORDON R., SMITH M. F., MAYNARD N. C., HEPPNER J. P., SPENCER N. W., WHARTON L., HAYS P. B. and KILLEEN T. L. 1986 *Planet. Space Sci.* **34**, 1.
- ST.-MAURICE J.-P. and SCHUNK R. W. 1979 *Rev. Geophys. Space Phys.* **17**, 99.
- ST.-MAURICE J.-P., HANSON W. B. and WALKER J. C. G. 1976 *J. geophys. Res.* **81**, 5438.
- SUVANTO K. 1987 *Planet. Space Sci.* **35**, 1429.
- WILLIS D. M., LOCKWOOD M., COWLEY S. W. H., VAN EYKEN A. P., BROMAGE B. J. I., RISHBETH H., SMITH P. R. and CROTHERS S. R. 1986 *J. atmos. terr. Phys.* **48**, 987.
- WINSER K. J., LOCKWOOD M. and JONES G. O. L. 1987 *Geophys. Res. Lett.* **14**, 957.